



OPEN ACCESS

EDITED BY

Jacob B. Lowenstern,
United States Geological Survey (USGS),
United States

REVIEWED BY

Tong Hou,
China University of Geosciences, China
Xing Ding,
Chinese Academy of Sciences (CAS),
China

*CORRESPONDENCE

Alessandra Correale,
✉ alessandra.correale@ingv.it

RECEIVED 12 December 2022

ACCEPTED 28 November 2023

PUBLISHED 03 January 2024

CITATION

Correale A, Corsaro RA, Miraglia L,
Paonita A and Rotolo SG (2024), The
December 2018 eruption at Etna
volcano: a geochemical study on melt
and fluid inclusions.
Front. Earth Sci. 11:1122132.
doi: 10.3389/feart.2023.1122132

COPYRIGHT

© 2024 Correale, Corsaro, Miraglia,
Paonita and Rotolo. This is an open-
access article distributed under the terms
of the [Creative Commons Attribution
License \(CC BY\)](https://creativecommons.org/licenses/by/4.0/). The use, distribution or
reproduction in other forums is
permitted, provided the original author(s)
and the copyright owner(s) are credited
and that the original publication in this
journal is cited, in accordance with
accepted academic practice. No use,
distribution or reproduction is permitted
which does not comply with these terms.

The December 2018 eruption at Etna volcano: a geochemical study on melt and fluid inclusions

Alessandra Correale^{1*}, Rosa Anna Corsaro², Lucia Miraglia²,
Antonio Paonita¹ and Silvio G. Rotolo^{1,3}

¹Istituto Nazionale di Geofisica e Vulcanologia, Sezione di Palermo, Palermo, Italy, ²Istituto Nazionale di Geofisica e Vulcanologia, Sezione di Catania, Catania, Italy, ³Dipartimento di Scienze della Terra e del Mare (DiSTeM), Università degli Studi di Palermo, Palermo, Italy

This study focus on the Mt Etna December 2018 eruption with the aim of investigating the geochemical characteristics of the feeding magma. New data on major and trace element geochemistry of olivine-hosted melt inclusions (MI) in volcanic products are presented together with the noble gas geochemistry of fluid inclusions (FI) in olivines. The noble gas geochemistry of fluid inclusions (FIs) in olivines was also investigated. The major element composition of MIs is variable from tephrite/trachybasalt to phonotephrite/basaltic trachyandesite, with $\text{SiO}_2 = 45.51\text{--}52.72$ wt%, $\text{MgO} = 4.01\text{--}6.02$ wt%, and $\text{CaO}/\text{Al}_2\text{O}_3 = 0.34\text{--}0.72$. Trace element patterns of MIs present a typical enrichment in LILE and LREE, depletion in HFSE, and relatively fractionated REE patterns: $(\text{La}/\text{Lu}) \text{N} = 18.8\text{--}41.08$, with $\text{Eu}/\text{Eu}^* = (0.5\text{--}1.8)$. Positive anomalies in Sr ($\text{Sr}/\text{Sr}^* = 0.8\text{--}2.3$) and Ba can be ascribed to the assimilation of plagioclase-rich cumulates in the magmatic reservoir. The variable Ba/La (9.8–15.8), K/Nb (260–1037), Ce/Nb (1.9–3.4), Rb/La (0.4–1.6), and Ba/Nb (10.8–25.8) ratios reveal mixing between two types of end-member magmas comparable to those emitted from 1) the 2001 Upper Vents and 2002–03 Northern Fissures (Type-1) and 2) the 2001 Lower Vents and 2002–03 Southern Fissures (Type-2), respectively. Type-2 represents a magma that was under the influence of a crustal component, whereas Type-1 is compatible with a HIMU–MORB-type heterogeneous mantle source. It appears that the 2018 MIs have captured the two different types of magmas, and the lack of homogenization may imply a very fast ascent (a few months). Compatible with the contemporary presence of primordial HIMU–MORB and crust-contaminated end-members are the data on noble gases from FI that highlighted an $^3\text{He}/^4\text{He}$ value of 6.5–6.6Ra. The hypothesis of two different types of magmas, identified by the trace element geochemistry in MIs, is, thus, reinforced by helium isotopic data on FI of the 2018 eruption together with data from other Etnean eruptions and allows the inference of a bicomponent magma mixing.

KEYWORDS

melt inclusions, fluid inclusions, trace elements, noble gases, Mt. Etna

1 Introduction

Mt. Etna is one of the most investigated and monitored volcanoes in the world and, due to frequent and well-sampled effusive and explosive eruptions, is represented as an excellent candidate for petrological and geochemical studies aimed at understanding the dynamics of magmatic processes from the source region to the surface.

Mt. Etna produces summit and flank eruptions that are largely controlled by magma ascent in the central conduits (e.g., Rittmann, 1965; Wadge, 1980; Ryan, 1988; Chester et al., 1985; Allard et al., 2006; Corsaro R. A. et al., 2009). In detail, summit eruptions occur at the open exit of the central conduits; they produce Strombolian explosions and lava fountains, often accompanied by lava flows. Flank eruptions, less frequent than the summit eruptions (Branca et al., 2004), are mostly driven by the fracturing of the central conduits and radial magma drainage and, in general, produce lava flows of a considerable volume (Branca and Abate, 2017).

In recent decades, the products of summit and most of the flank eruptions are highly porphyritic (porphyritic index, PI >20 vol%) and plagioclase-rich K-trachybasalts (Armienti et al., 1989; Corsaro and Pompilio, 2004; Métrich et al., 2004; Spilliaert et al., 2006; Viccaro et al., 2006; 2010; 2016; Corsaro et al., 2007; Corsaro et al., 2009; 2013; Ferlito et al., 2012; Giacomoni et al., 2012; 2014; 2016; Kahl et al., 2013; 2015; Corsaro et al., 2014; Mollo et al., 2015; 2018; Perinelli et al., 2016; Corsaro et al., 2017), which are stored in a shallow region of the volcano's plumbing system (<5 km b.s.L.; Métrich and Rutherford, 1998; Métrich et al., 2004). A limited number of flank eruptions (e.g., 1763, 1974, 2001, and 2002–03 in historic times) have been classified as being “eccentric” (Rittmann, 1965; Tanguy, 1980; Armienti et al., 1988). These are highly explosive eruptions and produce a nearly aphyric (PI <20% vol), plagioclase-poor, volatile-rich basaltic, K-trachybasaltic magma that ascends from a deep region (approximately 10–12 km b.s.L.; Spilliaert et al., 2006; Corsaro R. A. et al., 2009) bypassing the shallow plumbing system of the volcano. Interestingly, the highly porphyritic and aphyric type of magmas have contemporaneously erupted during the 2001 and 2002–03 flank eruptions, in particular from the Upper Vents (UVs) in 2001 and Northern Fissures (NFs) in 2002–03 and from Lower Vents (LVs) in 2001 and Southern Fissures (SFs) in 2002–03, respectively.

The eruption that happened on 24 December 2018 was a flank eruption that, interestingly, occurred approximately 10 years after the last flank activity of 2008–09. In particular, the eruptive activity at Mt. Etna resumed in the summer of 2018 with Strombolian explosions at Bocca Nuova (BN), North-East Crater (NEC), and South-East Crater (SEC), where lava effusions also occurred in August; weak Strombolian activity continued at BN, NEC, and NSEC (New South-East Crater) until 24 December. Starting from the morning of 24 December, thousands of shallow seismic events (Alparone et al., 2020; Giampiccolo et al., 2020) and the emission of an ash plume of up to 9 km a.s.l., from BN and NEC, heralded the opening of an eruptive fissure on the east flank of the SEC cone, which propagated downward for approximately 2 km. Several vents along the eruptive fissure fed a lava flow field that was covering an area of ≈ 1 km², until 27 December, when the eruption ended. The eruptive event of 2018 was the result of the intrusion of a dike; although the eruption was rather small, both in terms of the duration and extension of the lava flow, the entire event was accompanied by an intense seismic swarm with a considerable number of seismic events with a magnitude (M) >4 between 24 and 27 December (Alparone et al., 2020; Giampiccolo et al., 2020); the strongest one (M = 4.9) occurred on the night between 25 and 26 December (Alparone et al., 2020; Giampiccolo et al., 2020) and caused severe damage to the buildings of several villages on the southeastern flank of Etna.

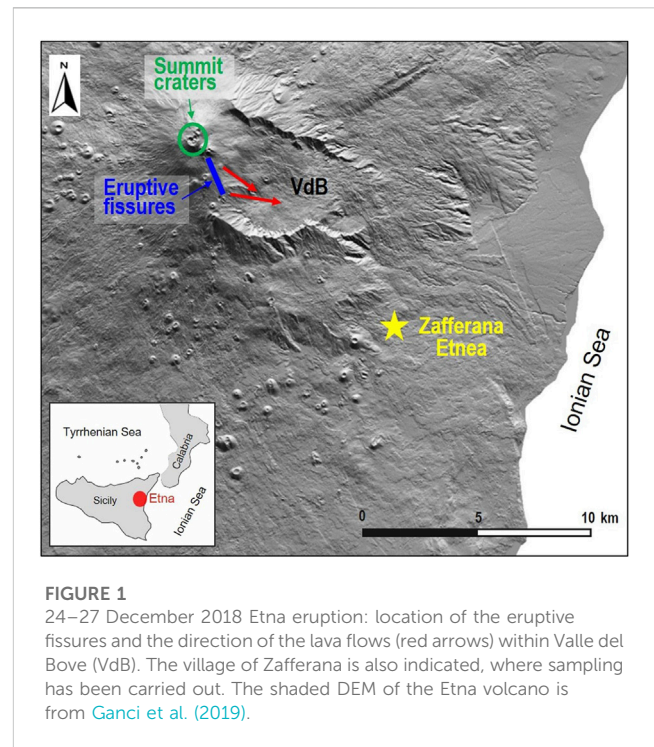


FIGURE 1
24–27 December 2018 Etna eruption: location of the eruptive fissures and the direction of the lava flows (red arrows) within Valle del Bove (VdB). The village of Zafferana is also indicated, where sampling has been carried out. The shaded DEM of the Etna volcano is from Ganci et al. (2019).

To date, this important eruptive event has been studied in a few articles (Alparone et al., 2020; Borzi et al., 2020; Giampiccolo et al., 2020; Paonita et al., 2021; Zuccarello et al., 2021; 2022), while the geochemistry was studied only with regard to free gas emissions (Paonita et al., 2021).

With the objective of better defining the features of the source and understanding the mechanisms that have driven the evolution of the primary magma related to this lateral event, we focused this study on the petrographic and petrological/geochemical characteristics of some representative samples of the eruption. In detail, we analyzed the major and trace element compositions of melt inclusions (MIs) entrapped in olivine phenocrysts that are particularly abundant in the products of this eruption. The information derived from the MIs geochemistry was integrated by a noble gas isotopic investigation of fluid inclusions (FIs) entrapped in olivine phenocrysts.

This study allowed us to recognize at least two compositional end-members, with one being more primitive, highlighting the occurrence of (shallower) crustal contamination that partially masked the characteristics of the source, and another being more evolved, representative of the typical magma feeding Mt. Etna's plumbing system.

2 Sampling and analytical methods

Analyses have been carried out on the material produced during the intense Strombolian activity that occurred at the eruptive fissures on 24 December 2018 that formed an ash cloud dispersed by the winds toward SE. In particular, we studied lapilli (# CSE 241218C) from the deposit sampled at Zafferana Etnea (Figure 1) which, due to rapid air quenching, was suitable for containing well-preserved melt inclusions.

The pyroclastic material was crushed, and olivine phenocrysts (0.5–1 mm in dimension) were separated by hand-picking under a binocular microscope and were attached to a microscope slide using Crystalbond™ resin and checked for melt inclusions using a polarizing microscope. The melt inclusions were selected on the basis of their 1) size, 2) shape, and 3) absence or a very limited degree of post-entrapment crystallization, preferably choosing those close to the phenocryst's core. In detail, the largest (>40 μm), most primitive, and poorly crystallized nine melt inclusions were chosen, polished, and analyzed for the major and trace element composition.

The major element composition of melt inclusions and hosting olivines was determined at the Istituto Nazionale di Geofisica e Vulcanologia Osservatorio Etneo (INGV-OE) using a LEO-1430 scanning electron microscope equipped with an Oxford EDS micro-analytical system (SEM-EDS). The analytical conditions are 20 kV and 1200 pA beam current (I Probe and XPP matrix correction method (Pouchou and Pichoir, 1986)). In order to minimize alkali loss during the analysis, a square raster of 10 microns was used. Analytical spots were chosen close to the rim (R) and core (C) of the olivine crystals and also in the proximity of the given melt inclusion. The accuracy of the measurements was checked through replicate analyses of the international standard VG-2 basaltic glass USNM 111240/52 and San Carlos olivine USNM 11131/444 (Jarosewich et al., 1980). The precision, expressed as the relative standard deviation, is less than 1% for SiO₂, Al₂O₃, FeO, MgO, and CaO and is less than 3% for TiO₂, MnO, Na₂O, K₂O, and P₂O₅ (Miraglia, 2012).

The trace element composition of melt inclusions and the hosting olivine was measured at the Istituto Nazionale di Geofisica e Vulcanologia, section of Palermo (INGV-PA) using a GeoLasPro 193 nm ArF Excimer laser ablation (LA) system, connected to an Agilent 7500ce quadrupole ICP-MS system. The analyses were performed with a constant laser repetition rate of 10 Hz, a fluency of 15 J/cm², and a He flux of 0.8 L/min in the ablation cell. Each analysis was carried out with a 32-μm spot, for a total analysis time of 2 min per spot, including 1 min of background acquisition time. The NIST 612 standard glass was used as an external standard and was measured at the beginning, in the middle, and at the end of each analytical sequence. ⁴³Ca, estimated by SEM-EDS, was used as the internal standard. The data were processed using the GLITTER program (Achterbergh et al., 2001). The accuracy of the analyses was calculated through repeated analyses of the USGS basaltic reference glass BCR-2G and resulted in being ≤15% for all the elements, except Ti and Tm, for which the accuracy was ≤20%. Precision was calculated through repeated analyses of the BCR-2 standard and resulted in being ≤20% for all the elements.

Noble gas measurements in FIs from olivine phenocrysts were carried out at ING-PA on aliquots of minerals that were previously cleaned using an ultrasonic bath with 6.5% HNO₃ before being rinsed with deionized water. The weight of the selected samples on average was 0.6 g. The amounts of elemental and isotopic He, Ne, and Ar in FIs were measured by single-step crushing under ultrahigh-vacuum conditions and at a pressure of approximately 200 bar. He and Ne were analyzed using two distinct Thermo Scientific Helix-SFT mass spectrometers, while Ar was analyzed using an Argus-GVI mass spectrometer. The analytical uncertainty (1σ) of the He-isotope ratio was <6.6%, while it was <3.7% and <8.3% for ²⁰Ne/²²Ne and ²¹Ne/²²Ne, respectively.

As usual, in noble gas studies (Graham, 2002; Martelli et al., 2011; 2014; Correale et al., 2016), the ⁴⁰Ar content of the samples was

corrected by assuming that all of the measured ³⁶Ar content was of atmospheric origin and was reported as ⁴⁰Ar*, whereas ³He/⁴He was corrected for atmospheric contamination using the approach presented in Giggenbach et al. (1993a) and is hereafter reported as Rc/Ra values (Rc and Ra being the ³He/⁴He ratios in the sample and in air, respectively).

3 Trace elements in MIs from Etna's recent eruptions

Many studies are focused on the MI content entrapped in the Etnean products (Kamenetsky and Clocchiatti, 1996; Metrich et al., 2004; Collins et al., 2009; Schiavi et al., 2015; Moretti et al., 2018; Gennaro et al., 2019), but only few of them investigated the trace element geochemistry in detail (Schiavi et al., 2015), probably owing to the difficulty of finding MIs in Etnean products and their small sizes, all the characteristics that make an accurate analysis of their trace element content difficult. In detail, Schiavi et al. (2015), by analyzing the trace element composition of some recent Etna eruptions (occurring from 2001 to 2006), identified three types of sources related to different geochemical characteristics:

- (i) **Type-1** (2001 Upper Vents, 2002 N): It is featured by REE, Y and Th enrichment, and lower ratios of LILE/REE, LILE/HFSE, and LILE/Th with respect to those of Type-2. This group lacks the negative HFSE anomaly, typical of subduction zone environments and features wide plagioclase crystallization and low potassium contents, showing an affinity with different types of magmas that have fed the pre-1971 eruptions. Furthermore, significant trace element ratios (e.g., K/La and Ba/Nb), along with Pb isotope data on Type-1 MIs, provide evidence for a composite heterogeneous mantle source (EM2 + DMM + HIMU).
- (ii) **Type-2** (2001 Lower Vents, LVs, 2002 S): It is characterized by lower concentrations of strongly incompatible elements (e.g., Nb, La, and Ce); by higher ratios of LILE/REE, LILE/HFSE, and LILE/Th with respect to those of Type-1; and by positive anomalies in Eu, Ba, and Sr. These MIs are interpreted as being produced by the interaction between the rising magma and cumulates of the plumbing system or with a plagioclase-rich crystal mush. Furthermore, some MIs of Type-2 show evidence of interactions with supercritical fluids from the deeper portions evidenced by K enrichment; it should be noted that both Type-1 and Type-2 MIs were present in olivines of the 2006 eruption, which highlighted the occurrence of mixing between Type-1 and Type-2 end-members.
- (iii) **Type-3** (2004 eruption): Similar to Type-2 MIs, this group is characterized by low K/Ba and high Ba/La and Ba/Nb ratios and K enrichment but differs from the former in its more important influence of the fractional crystallization process.

4 Results

4.1 Petrography

The studied lapilli are highly vesiculated scoriae (vesicles >50% vol.) with a porphyritic texture. Plagioclase is the most abundant

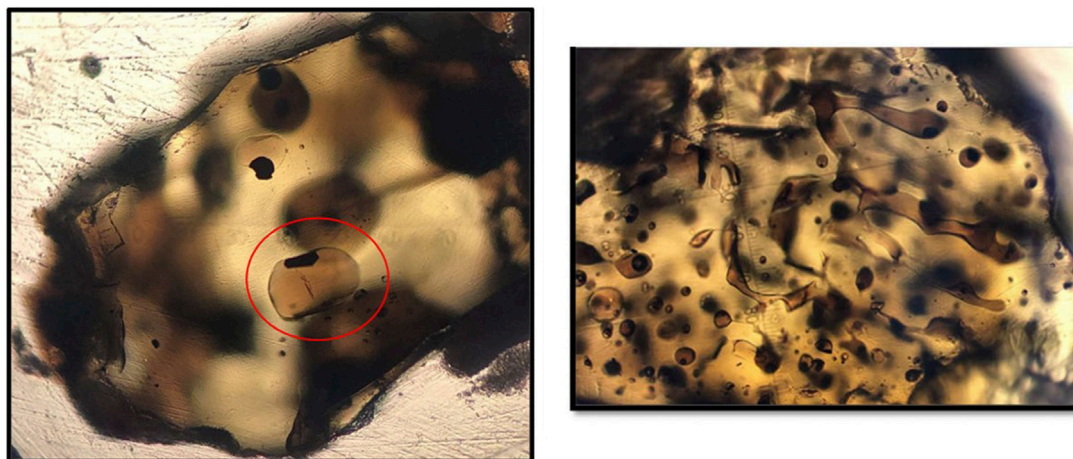


FIGURE 2
(A) Analyzed melt inclusions in the OL5 crystal, containing Fe and Mg oxides and **(B)** various melt inclusions in an olivine crystal.

TABLE 1 Average major element composition of olivines from the December 2018 eruption. The concentrations were recalculated to 100%. The totals are referred to the average, not normalized analyses. The major element data from the olivine core and rim are the best analyses selected on the basis of stoichiometry. The analyses were performed in the rim (R), core (C), and near the melt inclusion (MI).

	OL1		OL3			OL5			OL6		
	R	Near MI	R	C	Near MI	R	C	Near MI5-1	R	C	Near MI
		Ave			Ave			Ave			Ave
SiO ₂	37.84	37.76	37.94	37.99	37.83	37.98	37.63	37.75	38.22	37.99	38.14
FeO _{tot}	23.25	23.80	22.18	23.35	23.37	23.31	25.05	24.12	22.14	22.71	22.53
MnO	0.57	0.46	0.54	0.45	0.45	0.52	0.54	0.53	0.52	0.53	0.42
MgO	38.17	37.73	39.07	37.96	38.09	37.89	36.47	37.28	38.83	38.57	38.65
CaO	0.13	0.21	0.27	0.19	0.20	0.30	0.31	0.31	0.26	0.18	0.21
NiO	0.04	0.04	0.00	0.07	0.06	0.00	0.00	0.02	0.03	0.03	0.05
Total	98.64	99.94	100.52	100.64	100.18	99.95	99.58	97.50	100.52	99.80	100.18
Fo%	75.00	74.00	76.00	74.00	74.29	74.00	72.00	73.00	76.00	75.00	75.14
	OL10			OL15	OL17						
	R	C	Near MI	R	R	C	Near MI17-1	Near MI17-2	Near MI17-3		
			Ave				Ave	Ave	Ave		
SiO ₂	38.48	38.31	38.96	38.36	37.84	38.42	38.35	38.01	37.92		
FeO _{tot}	21.94	22.21	19.19	21.90	23.00	21.57	21.22	22.03	22.40		
MnO	0.46	0.48	0.35	0.53	0.49	0.42	0.39	0.42	0.53		
MgO	38.86	38.72	40.91	38.72	38.40	39.22	39.59	39.17	38.78		
CaO	0.26	0.28	0.45	0.30	0.28	0.37	0.37	0.34	0.35		
NiO		0.01	0.14	0.19			0.07	0.05	0.02		
Total	100.28	100.96	100.99	100.64	97.97	97.72	99.28	100.40	101.36		
Fo%	76.00	76.00	79.17	76.00	75.00	76.00	76.71	76.00	75.67		

phenocryst, followed by clinopyroxene, olivine, and Fe–Ti oxides; groundmass is glassy. Glomeroporphyritic aggregates formed by clinopyroxene and Fe–Ti oxides are common. Olivine phenocrysts from the studied products are particularly rich in melt inclusions (Figure 2), and characterized by their variable sizes from a few μm up to a hundred μm . Many MIs contain shrinkage bubbles, whereas only some of these include Fe–Ti oxides or are partially crystallized. In detail, we selected nine glass MIs, three of which were included in olivine #17. The selected MIs have regular sub-spherical shapes with a diameter of at least 40–50 μm .

4.2 Mineral chemistry

The major element composition of olivines is reported in Table 1. Each crystal was analyzed close to the rim and core and near the melt inclusions of interest. The selected olivine phenocrysts show slight normal zoning or in some cases are unzoned.

The compositional range (spots near the MIs) varies between Fo₇₂ in OL1 near M1 and Fo₇₉ in OL10 near MI1. If compared to the literature data (Schiavi et al., 2015; Gennaro et al., 2019), olivine phenocrysts from the 2018 eruption are akin to those that erupted during the more recent eruptions (Figure 3).

The composition of olivine can be related to the X_{Mg} of the melt with which the olivine is in equilibrium by an exchange distribution coefficient ($K_D^{\text{Fe-Mg}}_{\text{ol-liq}}$). This K_D is relatively constant in the range of magmatic pressure and temperature (Roeder and Emslie, 1970), though is known to have a dependence on melt composition due to non-ideal mixing of Fe and Mg in olivine and in the melt phase (Toplis, 2005). Taking into account the largely accepted values of $0.27 < K_D^{\text{Fe-Mg}}_{\text{ol-liq}} < 0.33$, almost all the cores and rims, as well as most of the near-MI olivine compositions, are in equilibrium with

the related MI composition, which is taken as a representative of the liquid composition.

4.3 Melt inclusions

4.3.1 Major elements

The major element data from melt inclusions are reported in Table 2 and shown in Figures 4, 5. In the table, we included the average composition of each melt inclusion after the correction for post-entrapment olivine crystallization (PEC). We carried out calculations following the method of Métrich and Clochiatti (1996), assuming an olivine–melt equilibrium Mg–Fe exchange partition coefficient ($K_D^{\text{Fe-Mg}}_{\text{ol-liq}}$) of 0.30, which we prefer to maintain for achieving homogeneity with the values previously used for Etna mafic magmas ($K_D^{\text{Fe-Mg}}_{\text{ol-liq}} = 0.29\text{--}0.30$; Métrich and Clochiatti, 1996; Giacomoni et al., 2014; Schiavi et al., 2015; Gennaro et al., 2019; Zuccarello et al., 2022). PEC correction was in the range 1.3 and 4.9 wt%, with the highest and the lowest values being applied in M1 from OL1 and in M2 from OL17, respectively. Considering that the calculated PEC are < 5 wt%, its effects on incompatible elements will be negligible (Rose-Koga et al., 2021).

In the TAS diagram (Le Maitre, 2002), the results of the major element composition of melt inclusions are rather variable from tephrite/trachybasalt to phonotephrite/basaltic trachyandesite (Figure 4), with the OL10M1 (on average $\text{SiO}_2 = 45.51$ wt%; $\text{Na}_2\text{O} + \text{K}_2\text{O} = 5.52$ wt%) and OL1MI (on average $\text{SiO}_2 = 52.72$; $\text{Na}_2\text{O} + \text{K}_2\text{O} = 8.01$ wt%) melt inclusions representing the most primitive and evolved terms, respectively. On the whole, the studied MIs fall within the field of recent eruptions (green field in Figure 4) and show a particular similarity with the products from the 2001 and

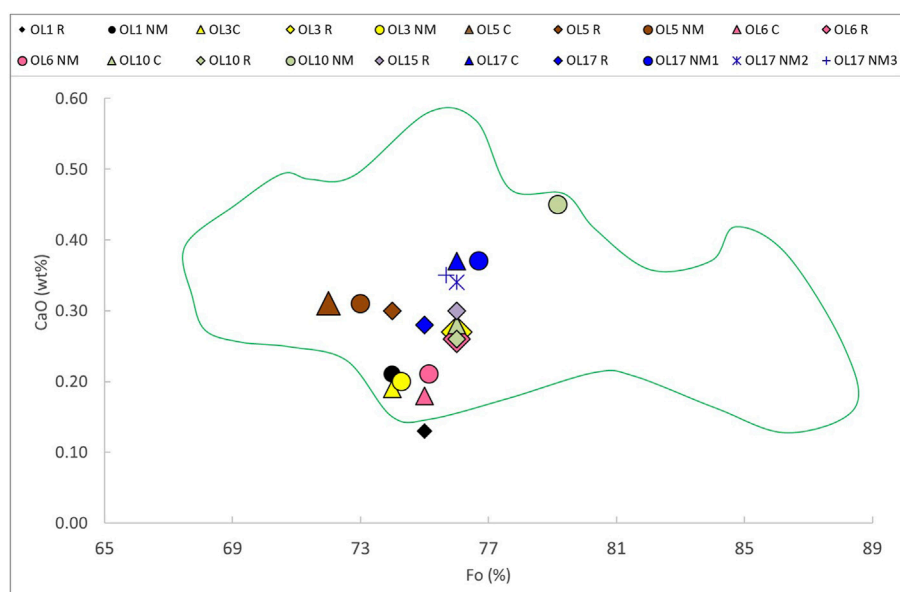
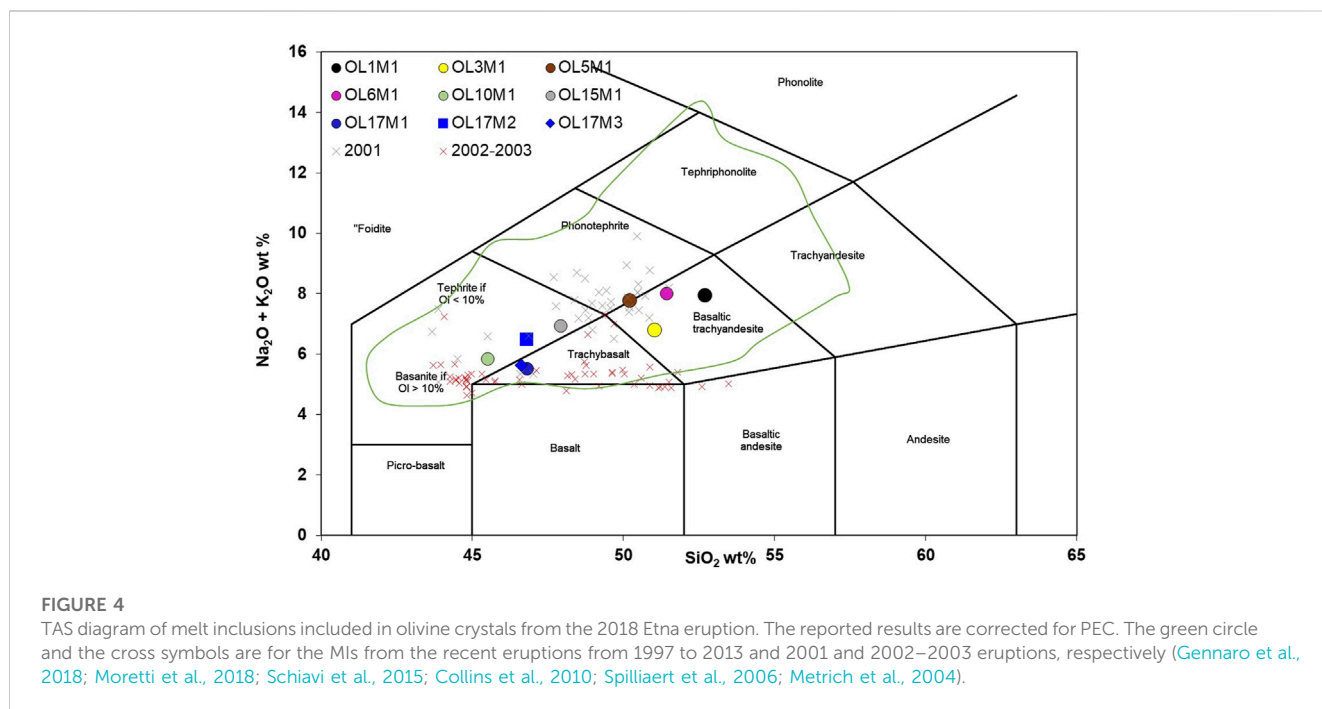


FIGURE 3

CaO vs. Fo content of olivine crystals from the 2018 Etna eruption. The green line represents the field of literature data from recent Etna eruptions and is obtained from Schiavi et al. (2015), Gennaro et al. (2018), and Borzi et al. (2020).

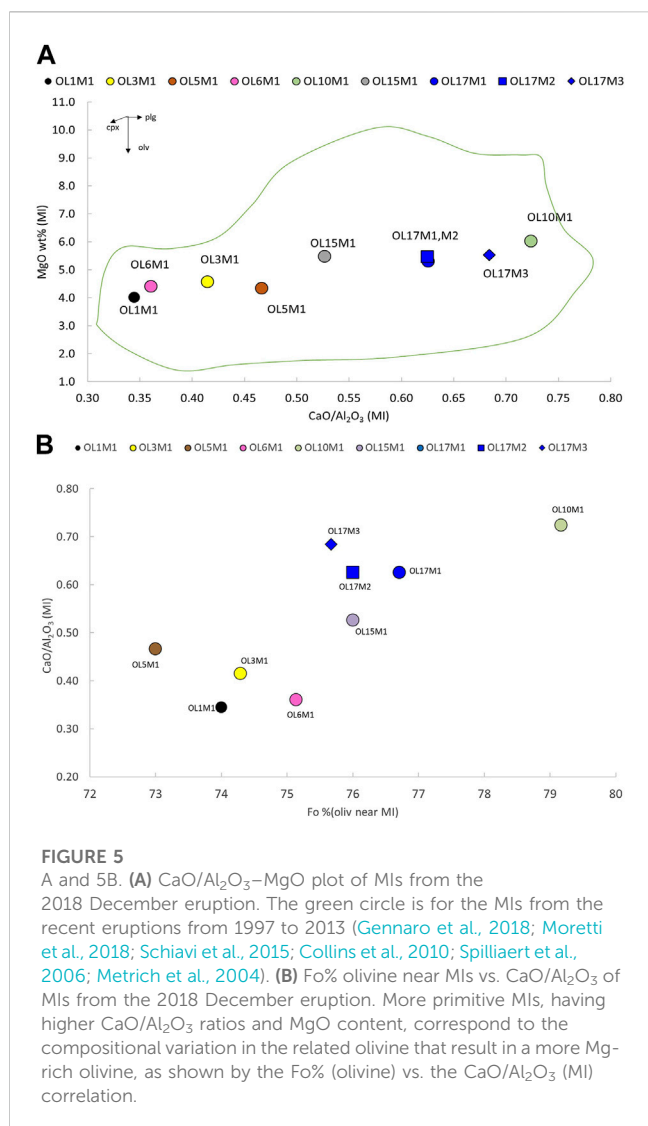
TABLE 2 Average major element composition of melt inclusions in olivines from the December 2018 eruption. The concentrations were recalculated to 100% and were corrected for PEC, following the method of **Métrich and Clochiatti (1996)** and assuming a value ($K_D^{Fe-Mg_{ol-liq}}$) of 0.30. The totals are referred to the average, not normalized analyses. Mg_v^* = molar MgO/MgO + FeO; fixing a Fe_2O_3/FeO ratio = 0.20.

Host olivine	OL1	OL3	OL5	OL6	OL10	OL15	OL17		
MI Label	OL1M1	OL3M1	OL15M1	OL6M1	OL10M1	OL15M1	OL17M1	OL17M2	OL17M3
No. of analyses	13	11	17	5	13	6	23	8	5
SiO ₂	52.72	51.04	50.22	51.44	45.51	47.93	46.82	46.78	46.61
TiO ₂	1.54	1.82	1.69	1.71	1.91	1.63	0.92	1.71	1.71
Al ₂ O ₃	17.95	17.69	17.20	18.06	17.37	17.61	18.70	17.08	16.77
FeO _{tot}	9.51	10.54	10.52	9.65	10.59	10.94	10.64	11.55	12.02
MnO	0.14	0.21	0.23	0.21	0.19	0.20	0.19	0.24	0.25
MgO	4.01	4.56	4.34	4.40	6.02	5.47	5.30	5.47	5.54
CaO	6.19	7.34	8.02	6.51	12.57	9.27	11.70	10.68	11.47
Na ₂ O	5.16	4.60	4.76	5.58	3.40	3.78	3.28	3.49	3.21
K ₂ O	2.78	2.18	3.00	2.43	2.43	3.16	2.24	3.01	2.43
Total	101.10	101.22	101.20	101.11	101.21	101.25	101.18	101.32	101.38
Mg _v [*]	47.04	47.66	46.43	48.99	54.43	51.26	51.13	49.90	49.22
PEC	0.019	0.021	0.032	0.022	0.040	0.032	0.029	0.037	0.037



2002 eruptions. Furthermore, in the MgO vs. CaO/Al₂O₃ plot (see **Figure 5A**), the end-members of compositional variability are represented by OL1M1 and OL10M1, featured by MgO ranging from 4.01 to 6.02 wt% and CaO/Al₂O₃ varying from 0.34 to 0.72, respectively. It is important to note that the presence of more primitive melts (trapped as MIs in olivine phenocrysts), having higher CaO/Al₂O₃ ratios and MgO content (**Figure 5A**),

corresponds to compositional variations in the adjacent olivine that results in a more Mg-rich olivine, as shown by the Fo% (olivine) vs. the CaO/Al₂O₃ (MI) correlation plotted in **Figure 5B**. Finally, MI from the December 2018 eruption falls in the literature field (green circle in **Figure 5A**), sampling the whole compositional variability of the literature (1999–2013 eruptions).



4.3.2 Trace elements

The trace element compositions of the products from the 2018 eruption are reported in Table 3 and are shown in Figures 6-8. The analyzed melt inclusions show variable trace element concentrations (Table 4), with OL17M1 and OL3M1 showing the highest and lowest concentrations, respectively.

The spider diagram of Figure 6 demonstrates 1) a more pronounced enrichment in the fluid mobile elements over HFSE and HREE than that of a typical OIB (Sun and McDonough, 1989); 2) high LILE and LREE concentrations, similar to the post-1971 lavas (Tonarini et al., 2001; Metrich et al., 2004; Viccaro and Cristofolini, 2008); and 3) a similarity with the Type-2 source of Schiavi et al. (2015). Furthermore, a simultaneous positive anomaly of Ba, Sr (Sr/Sr* ranging from 2.3 in OL17M1 to 0.85 in OL1M1), and Eu (Eu/Eu* of up to 1.8 in OL10M1) is highlighted.

Figure 7 shows Ba/La vs. 1/La and K/Nb vs. 1/Nb, allowing the identification of variabilities in Ba/La (9.8–15.8) and K/Nb (260–1037), where the extreme values correspond to OL3M1 and OL17M2, respectively, as minimum values, and OL17M1 as maximum values. Figure 8 shows the Rb/La vs. Ce/Nb and Rb/La vs. Ba/Nb plots, indicating the compositional variability of MIs from

1.9 to 3.4 for Ce/Nb, from 0.4 to 1.6 for Rb/La, and from 10.8 to 25.8 for Ba/Nb, where the extreme values of the dataset coincide with those from OL17M2/OL3M1 and OL17M1 for the minimum and maximum values, respectively.

4.4 Noble gases in fluid inclusions

The gas content released by the crushing technique and analyzed for noble gases is mainly obtained from gas bubbles entrapped in the minerals, although we cannot exclude the fact that a part of it comes from the shrinkage bubbles of MIs. The He concentration ranges between 6.16 and 7.05 × 10⁻¹³ mol/g and is coherent with the eruptive history of Etna from the literature (see Figure 9). The R/Ra value varies between 6.5 and 6.6 Ra and is also, in this case, in the range of 4.9 and 8.2 Ra, which is given in the literature data (Marty et al., 1994; Nuccio et al., 2008; Correale et al., 2014).

The ²⁰Ne, ²¹Ne, and ²²Ne concentrations vary between 7.8 and 4.1 × 10⁻¹⁵, 2.6 and 1.4 × 10⁻¹⁷, and 7.9 and 4.2 × 10⁻¹⁶ mol/g, whereas the ²⁰Ne/²²Ne and ²¹Ne/²²Ne ratios are 10, 9.9, and 0.033, respectively (Table 4). The elemental concentrations of ⁴⁰Ar and ³⁶Ar vary between 1.5 and 1.6 × 10⁻¹², and 5.4 and 5.2 × 10⁻¹⁵, respectively, whereas the ⁴⁰Ar/³⁶Ar ratio is between 302.5 and 307.5, highlighting the presence of an important atmospheric contaminant.

5 Discussion

5.1 Magmatic environment of origin as inferred by the olivine composition

Borzi et al. (2020) distinguished between two different types of olivines in the 24–27 December 2018 flank eruption at Mount Etna: 1) the first type represents the dominant one (approximately 76% of olivine phenocrysts) and is featured by olivines normally or is reverse-zoned, whereas 2) the second one (~24% of the observed phenocrysts) is almost unzoned or characterized by very tiny Fo oscillations, in the order of ~1 Fo mol%. The first type of olivines also includes phenocrysts with thin-zoned (6 to 7 μm wide) rims characterized by abrupt Fo decreases to Fo₇₂₋₇₅ or thick-zoned rims (up to 50 μm wide), along with the Fo content decreasing gradually to Fo₆₆₋₇₂ or Fo₇₈, whereas the composition of the second olivine type is mostly in the range Fo₇₅₋₇₆ and Fo₇₇₋₇₈. Zuccarello et al. (2021, 2022) also reported olivine core and rim compositions from the same 2018 eruption, ranging from Fo₇₄ to Fo₈₄ and from Fo₇₄ to Fo₇₉, respectively. The olivine crystals from the tephra deposits investigated in the present study reported a more limited range with respect to that presented by both Borzi et al. (2020) and Zuccarello et al. (2021, 2022) and show a greater similarity with the second category defined by Borzi et al. (2020), being almost unzoned and having Fo mol% contents comparable to those measured by Borzi et al. (2020) for this compositional/petrographic type.

The first goal of our research was to investigate the pressure from which different types of magmas originate from, referring to the compositional magmatic horizons defined in previous studies. Giuffrida & Viccaro (2017) distinguished between five compositionally distinct magmatic environments (Mi), whose

TABLE 3 Average trace element analyses of MIs entrapped in olivine crystals from the 2018 December eruption. Each analysis was carried out with a 32- μm spot and is associated with an accuracy and precision lower than 15% for most of the elements. A number of analyses variable between 1 and 3 were carried out as a function of the MI size.

Host olivine	OL1	OL3	OL5	OL6	OL10	OL15	OL17		
MI Label	OL1M1	OL3M1	OL5M1	OL6M1	OL10M1	OL15M1	OL17M1	OL17M2	OL17M3
No. of analyses	2	2	2	1	2	1	4	1	1
ppm									
Li	17.27	14.57	15.68	18.86	10.13	9.83	13.79	3.30	13.60
Be	2.11	2.42	2.52	1.91	2.23	<0.54	1.20	5.29	2.13
B	24.31	16.40	15.74	18.35	17.36	16.03	6.10	18.37	10.46
Sc	13.74	13.58	16.19	14.80	28.54	19.73	19.29	20.59	22.91
Ti	9,193.54	10,380.40	10,041.13	10,356.83	11,651.40	15,135.15	5,246.35	9,664.92	9,062.32
V	176.33	195.80	221.02	191.67	337.86	bdl	138.74	265.46	238.64
Cr	bdl	11.97	4.38	bdl	7.93	bdl	7.62	bdl	9.02
Mn	1,269.02	1,598.47	1,644.51	1,934.37	1,467.83	2,145.49	1,427.91	1,456.49	1,697.66
Co	28.42	45.66	29.54	101.31	42.56	96.32	39.62	45.25	41.31
Ni	8.68	28.11	7.59	213.10	34.92	123.95	18.23	33.37	30.49
Cu	129.12	84.11	155.08	7,244.43	76.26	78.49	109.11	66.99	76.65
Zn	111.58	136.39	120.33	178.41	147.22	212.13	122.30	136.32	156.45
As	4.72	3.24	2.86	4.72	1.43	3.06	1.29	3.82	1.89
Rb	55.08	40.12	72.91	45.00	69.09	65.08	58.58	74.85	56.49
Sr	1,052.67	1,592.77	1,328.10	1,718.30	1,392.07	1,952.04	1,383.18	1,555.54	1,346.93
Y	23.74	30.93	29.30	28.01	25.60	24.92	14.85	21.30	23.49
Zr	228.29	214.19	238.63	235.62	183.93	277.41	67.89	295.65	180.86
Nb	80.68	69.62	65.48	76.63	42.89	74.10	22.23	89.45	42.49
Cs	1.12	0.94	1.28	0.97	1.07	1.22	0.89	1.60	0.85
Ba	1,063.78	1,067.72	873.75	1,122.63	633.92	1,102.67	570.14	972.03	632.62
La	93.71	107.14	78.78	105.24	53.11	101.32	36.85	98.86	54.43
Ce	174.39	213.68	147.22	212.12	107.79	186.58	75.45	176.70	110.26
Pr	18.22	23.61	16.04	22.58	12.43	19.78	8.55	18.11	12.79
Nd	64.99	89.47	59.25	84.62	48.17	62.66	32.65	56.10	49.55
Sm	10.65	14.35	10.54	12.00	9.38	9.89	5.73	9.22	10.05
Eu	2.77	3.88	3.11	3.23	3.01	2.96	2.05	2.53	2.87
Gd	8.03	10.58	8.90	8.91	8.11	9.51	4.58	6.69	8.11
Tb	0.93	1.24	1.09	1.08	1.02	0.84	0.56	0.68	0.99
Dy	4.79	7.14	6.20	6.24	5.63	5.73	3.20	4.98	5.77
Ho	0.92	1.25	1.15	1.14	1.01	0.93	0.58	0.80	1.07
Er	2.31	2.99	2.81	2.80	2.52	2.62	1.44	2.00	2.62
Tm	0.30	0.43	0.39	0.30	0.35	0.41	0.19	0.22	0.34
Yb	2.31	2.83	2.60	2.66	2.18	2.56	1.25	2.34	2.16
Lu	0.33	0.43	0.41	0.27	0.30	0.32	0.17	0.26	0.28

(Continued on following page)

TABLE 3 (Continued) Average trace element analyses of MIs entrapped in olivine crystals from the 2018 December eruption. Each analysis was carried out with a 32- μm spot and is associated with an accuracy and precision lower than 15% for most of the elements. A number of analyses variable between 1 and 3 were carried out as a function of the MI size.

Host olivine	OL1	OL3	OL5	OL6	OL10	OL15	OL17		
MI Label	OL1M1	OL3M1	OL5M1	OL6M1	OL10M1	OL15M1	OL17M1	OL17M2	OL17M3
No. of analyses	2	2	2	1	2	1	4	1	1
ppm									
Hf	4.89	4.50	4.98	4.20	4.10	5.45	1.27	5.94	4.20
Ta	3.73	3.30	3.19	3.68	2.03	3.54	0.82	3.97	2.22
Pb	11.88	7.60	9.71	28.48	6.89	9.59	5.85	8.65	6.27
Th	15.68	13.01	10.63	13.08	6.06	14.68	2.89	14.69	6.65
U	4.73	4.03	3.04	4.05	2.03	4.55	1.02	4.90	2.23

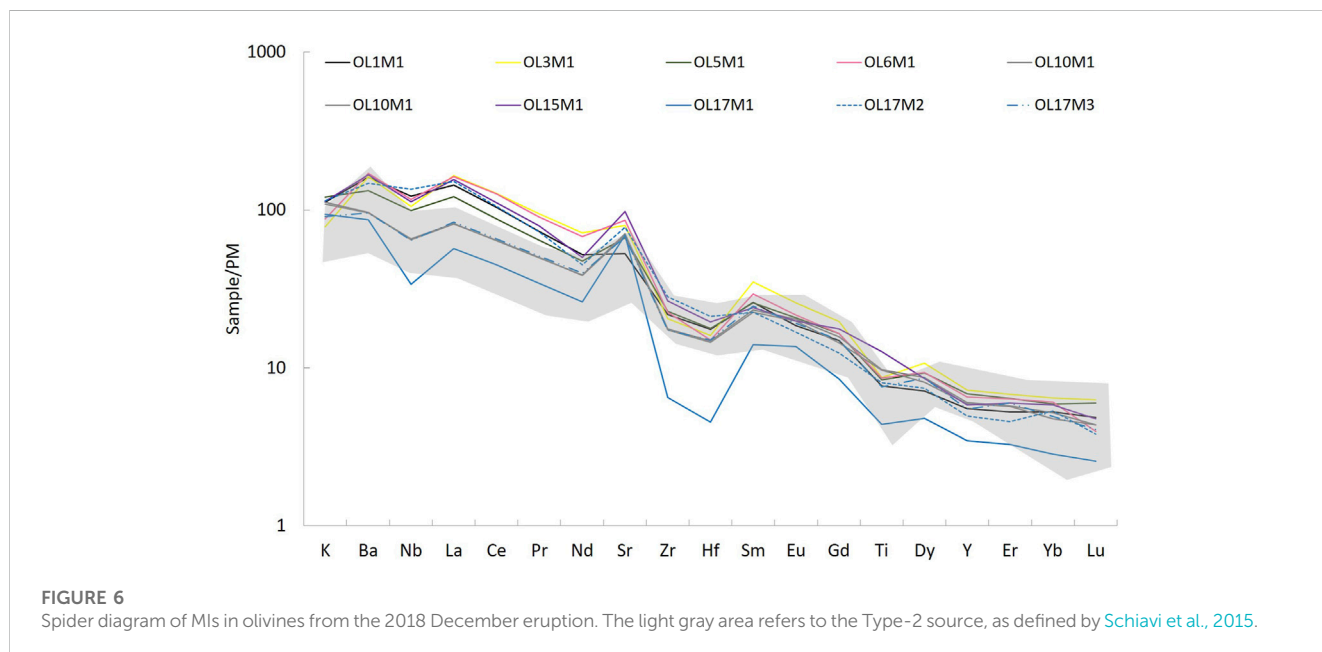


FIGURE 6 Spider diagram of MIs in olivines from the 2018 December eruption. The light gray area refers to the Type-2 source, as defined by Schiavi et al., 2015.

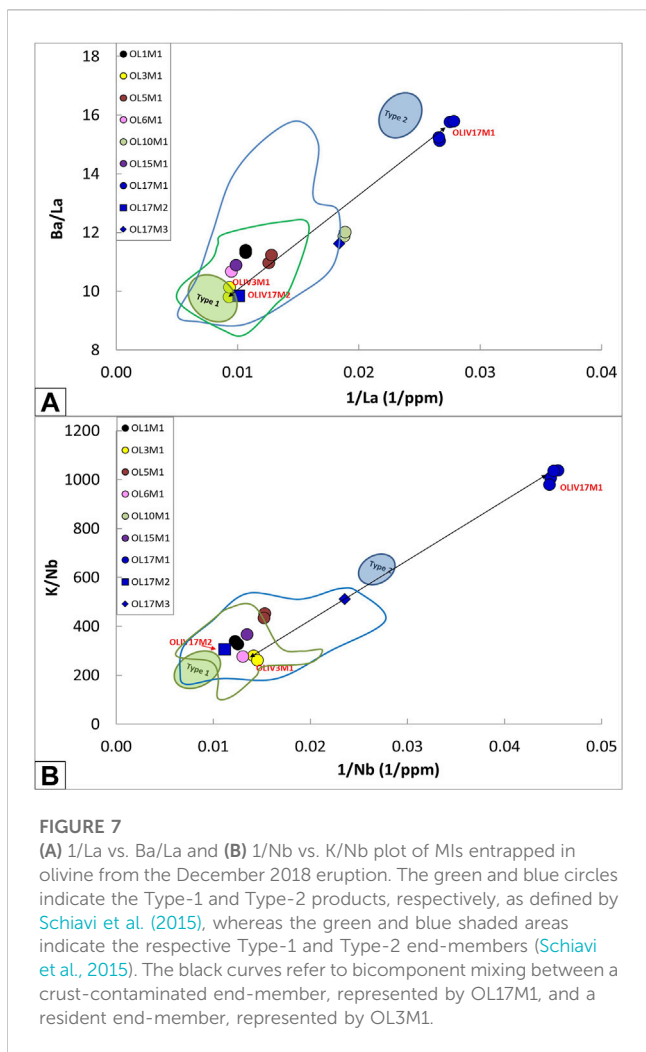
pre-eruptive P–T– $f\text{O}_2$ conditions, including volatile concentrations, were constrained by thermodynamic modeling on the basis of the forsterite content found in the olivine cores from 2011 to 2013 eruptive activity. In detail, the authors distinguished between the following: 1) the deepest reservoir M00, located at ~600 MPa and characterized by Mg-rich olivine phenocrysts (Fo_{84}); 2) an M0 level at ~390 MPa with Fo_{80-82} olivines; 3) M1a (Fo_{78} ; 250 MPa) and M1b (Fo_{75} ; ~140 MPa) levels; and 4) finally, the shallow M2 (Fo_{70-73} ; ~40 MPa) storage zones.

Starting from the classification in Giuffrida & Viccaro (2017), Borzi et al. (2020) highlighted that most crystal cores from the eruption of 24 December 2018 crystallize at pressures of 290–230 and 160–120 MPa, reflecting magma storage and differentiation in the conditions of the M1a and M1b environments, respectively. Furthermore, the olivine rim composition from the same eruption suggests a re-equilibration at shallow pressure (≤ 30 MPa), which reflects the thermodynamic conditions of M2. Coherently with Borzi et al. (2020), the loose

tephra of the December 2018 eruption investigated in this study are attributable to the same inferred reservoirs (that is M1a, M1b, and M2), allowing us to constrain the pressure of two end-members identified by the major and trace element geochemistry at approximately 40 MPa for the shallower and more evolved magma, and at approximately 140–250 MPa for the deeper and crust-contaminated term.

5.2 Magma evolution and mixing processes as evidenced by the major and trace element geochemistry

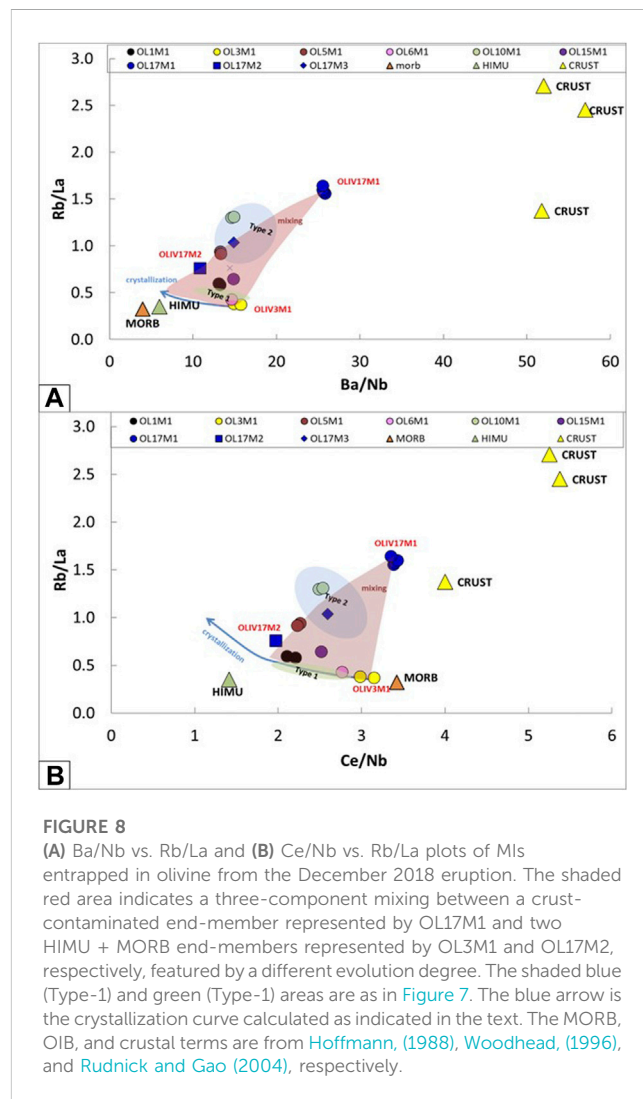
We tested if the wide compositional variability highlighted by major elements in the MIs embedded in 2018 lapilli (see Section 4.3.1) could be explained through a fractional crystallization process. It would involve parental and residual liquids with the compositions of the most primitive (OL10M1) and the most evolved (OL1M1)



melt inclusions, respectively, which fractionate plagioclase, clinopyroxene, olivine, and Ti-magnetite.

Mass balance calculations indicate that it is necessary to remove 24% clinopyroxene ($Wo_{49}En_{38}Fs_{12}$), 24% plagioclase (An_{83}), 7% Ti-magnetite, and 2% olivine (Fo_{82}) to match the observed compositional variability. The unrealistically high amount of crystal fractionation needed (57 wt%), coupled with the bad fit (sum of the square residuals = 4) between the modeled and real contents of major oxides, suggests that a simple FC process is not suitable for explaining the compositional variability between the MIs of OL10 and OL1.

Consequently, we have to hypothesize an additional process to explain the compositional variations. Following this reasoning, we assume a mixing between a melt rising from the depths during a recharge phase with the resident magma in a shallower reservoir. The more primitive end-member would be higher in MgO, CaO/ Al_2O_3 , and lower alkali and silica contents, whereas the more evolved end-member (the resident magma) should be characterized by lower MgO and CaO/ Al_2O_3 and higher alkali and silica contents. Evidence of this process might be found in MIs in olivine phenocrysts, which record the occurrence of both melt types that are in close agreement with the compositional variations in the corresponding (nearby MIs) olivine (see Figure 5B).



The trace element geochemistry also highlights a certain variable composition (see section 4.3.2), which, in any case, cannot be entirely explained through crystallization processes (see blue curves in Figures 8A,B, respectively).

The fractional crystallization process was simulated using the equation of White (2005). Starting from the bulk partition coefficients of White (2005), we calculated the bulk partition coefficients of the i element with the weighted mean of the mineral content in the studied rocks (olivine, 20%; plagioclase, 48%; and clinopyroxene, 32%). The used C_0 are from OLIV3M1 that represents the MIs with the highest/more primitive Ce/Nb and Ba/Nb ratios. The rapid decrease in Ce/Nb and Ba/Nb, calculated for the crystallization process, is a consequence of the different D values obtained for Nb (1.84×10^{-2}) with respect to those calculated for Ba and Ce (1.59×10^{-1} and 6.91×10^{-2} , respectively). This evidence supports our speculation about a mixing between two different types of magmas with different geochemical characteristics. The black mixing curves, represented in Figure 7, enable us to explain the variability of K/Nb and Ba/La ratios in the analyzed products. They were calculated while considering the average values of K/Nb and Ba/La ratios and the average 1/La and 1/Nb

TABLE 4 Isotopic and elemental noble gas compositions from olivine crystals of the 2018 December Etnean eruption. The gas content analyzed for He, Ne, and Ar was obtained from fluid inclusions entrapped in the minerals and was extracted by the crushing technique (see text).

Sample	Mineral	⁴ He 10 ⁻¹³ mol/g	⁴ He err	²⁰ Ne 10 ⁻¹⁵ mol/g	²⁰ Ne err	²¹ Ne 10 ⁻¹⁷ mol/g	²¹ Ne err	²² Ne 10 ⁻¹⁶ mol/g	²² Ne err
ET2018	Olivine	7.05	0.02	7.79	0.75	2.56	2.23	7.92	0.78
ET2018	Olivine	6.16	0.02	4.15	0.86	1.41	2.67	4.19	0.93
⁴⁰ Ar 10 ⁻¹² mol/g	⁴⁰ Ar err	⁴⁰ Ar*10 ⁻¹⁴ mol/g	⁴⁰ Ar* err	He/Ne	Err %	R/Ra	Rc/Ra	Err tot +/-	
1.62	0.07	3.62	0.10	90.49	0.749	6.48	6.5	0.09	
1.54	0.07	0.99	0.09	148.33	0.860	6.61	6.6	0.09	
⁴⁰ Ar/ ³⁶ Ar	Err (%)	²⁰ Ne/ ²² Ne	Err tot +/-	²¹ Ne/ ²² Ne	Err tot +/-				
307.5	0.07	10.05	0.04	0.03	0.00				
302.5	0.05	9.87	0.05	-	-				

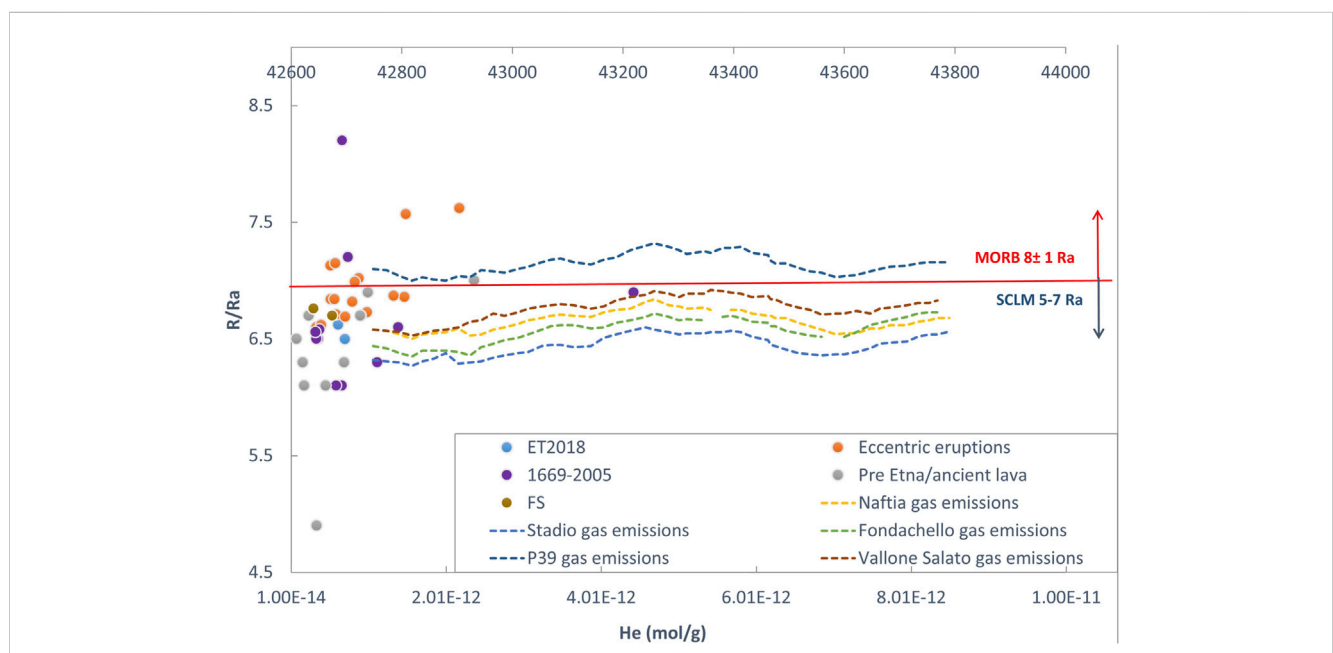


FIGURE 9 He concentrations vs. ³He/⁴He (reported as R/Ra) of fluid inclusions entrapped in olivine crystals from the 2018 eruption. The literature data (only FIs from olivine crystals) are plotted for comparison and are obtained from Marty et al. (1994), Nuccio et al. (2008), and Correale et al. (2014). The MORB and SCLM fields are from Graham (2002) and Dunai and Porcelli (2002), respectively. The gas emissions collected from five different sampling sites (Naftia, Stadio, Fondachello, P39, and Vallone Salato; Caracausi et al. (2003)) are also plotted for comparison, as a function of time, and are reported with dashed lines.

concentrations of OL3M1 and OL17M1 as minimum and maximum end-members, respectively. These values are comparable to Type-1 and Type-2 magmatic components studied by Schiavi et al. (2015), respectively.

Furthermore, the red mixing area in Figure 8 shows that the measured trace element variability of Rb/La, Ce/Nb, and Ba/Nb ratios is compatible with a three-component mixing, where the three end-members coincide with OL17M1, OL3M1, and OL17M2. Interestingly, the three terms present a similarity with the Type-1

(OL3M1 and OL17M2) and Type-2 (OL17M1) magmatic components from Schiavi et al. (2015).

The simultaneous positive anomalies of Ba, Sr, and Eu (see Figure 6 and Section 4.3.1) could be related to the assimilation processes of plagioclase accumulated in the magma chamber (Sobolev et al., 2000), while the negative Nb anomaly could be tied to crustal involvement. Indeed, the interaction between a mafic melt with ol + plg produces an aluminum-rich spinel and a modified melt with typical positive anomalies of Ba, Sr, and Eu

(Danyushevsky et al., 2004). Similarly, Schiavi et al. (2015) observed the occurrence of plagioclase assimilation in some glassy inclusions entrapped in olivines from recent eruptions (2001 LV and 2002 S). These latter authors also infer that a melt inclusion contained a plagioclase crystal which showed traces of reaction and melting, suggesting that plagioclase had not crystallized from entrapping MIs, but was already present before its formation.

As discussed in Section 3 and, subsequently, in Section 5.2, the Type-2 population is contaminated by a crustal component. This contamination could, at least in part, occur in the form of assimilation, as suggested by Schiavi et al. (2015), although other ways (e.g., diffusion processes) cannot be excluded. Consequently, the higher the amount of the crustal contaminated end-member involved in mixing, the higher the measured K/Nb, Ba/La Rb/La, Ce/Nb, and Ba/Nb ratios will be.

At this point, we inquire into the correspondence between the major and trace element geochemistry with regard to the end-members defined above. In detail, data suggest that the group of MIs with a more primitive major element composition (OL10M1, OL17M1, OL17M2, and OL17M3) is coupled with a more marked crustal nature, as evidenced by trace elements. Conversely, the MI group, showing more evolved characteristics of major elements (OL1M1, OL3M1, OL6M1, and OL5M1), is also the one in which the trace elements highlighted a more primordial signature. This evidence is in agreement with the interpretation according to which deep magma rises from the depths and is contaminated by the crustal material before being mixed with magma ponding in the Etnean reservoir in the shallower area of the reservoir. Following this interpretation, the trace elements that are more sensitive geochemical tracers with respect to major elements record the crustal contamination event, whereas the major elements geochemistry would keep track of the more primitive signature of the deep magma. In the following section, we clarify some details on the nature of mixing end-members.

5.3 Magma source features and possible crustal involvement

By comparing the values measured in the MIs of the 2018 eruption with typical HIMU–OIB and MORB sources and with a crustal component, it is possible to speculate that OL17M1 could be representative of magma that underwent some degree of crustal contamination when compared to the melt inclusions entrapped in OL3M1 and OL17M2. Therefore, referring to the mixing process discussed in the previous section, we propose that an end-member higher in Ba/Nb and Rb/La ratios, represented by OL17M1, was mixed, at different degrees, with melts that originated in the HIMU + MORB heterogeneous mantle source (already recognized by isotopic systematics by Correale et al., 2014; Schiavi et al., 2015; etc.) after undergoing crystal fractionation.

An alternative interpretation here could be that two primitive end-members from the mantle source coexist, each of them with distinct proportions of the MORB and HIMU components. In this latter case, the variability of the entire dataset would be reproduced by mixing of a fixed crust-contaminated term (OL17M1) and melts that originated in

the variable HIMU + MORB heterogeneous mantle source. Clearly, following this hypothesis, the role of the crystallization process on the variable composition of the dataset would be marginal, which is, nevertheless, evident from major elements. Indeed, it is difficult to imagine that melt inclusions entrapped in olivines from the same eruption are related to different proportions of HIMU and MORB end-members from the source.

In the Etnean volcanic system, the presence of the composite HIMU/FOZO + DMM mantle source (Viccaro and Cristofolini, 2008; Correale et al., 2014; Schiavi et al., 2015; Di Renzo et al., 2019), as well as a “fossil” magmatic component related to the interaction of the melt with plagioclase-rich cumulates or crystal mushes, was previously suggested by different authors (Schiavi et al., 2015).

The occurrence of chemically distinct MIs in phenocrysts from a single eruptive event, or even within a single phenocryst, is not unique to the Etnean volcanic system, which was also evidenced by Schiavi et al. (2015) and has been found in various geodynamic settings [e.g., Sobolev and Shimizu, 1993; Gurenko and Chaussidon, 1995; Sobolev, 1996; Danyushevsky et al., 2004].

In the specific case of the December 2018 eruption, the variable compositions of MIs indicate that a HIMU + DMM heterogeneous mantle originated in melts that evolved through fractional crystallization in crustal reservoirs and mixed with a magma with some degree of crustal contamination (or plg assimilation as highlighted by the high number of Ba and Sr positive anomalies) stored in the plumbing system.

The coexistence of different melt compositions trapped within olivines from the same eruption was probably due to a lack of homogenization in a highly heterogeneous plumbing system, possibly a consequence of the fast ascent of the magma batch, as recently documented by Zuccarello et al. (2022) for the December 2018 eruption.

5.4 Noble gases

5.4.1 Isotopic helium of the December 2018 eruption in the context of the literature data

Isotopic helium from the 2018 eruption shows a variability ranging between 6.5 and 6.6 Ra, which perfectly coincides with that measured from the literature ($R_c/R_a = 4.9\text{--}8.2$; Figure 9). Considering that the FIs from pyroxenes are, on average, featured by lower $^3\text{He}/^4\text{He}$ ratios as a consequence of their later crystallization with respect to that of olivines (Marty et al., 1994; Hilton et al., 1995; Shaw et al., 2006; Nuccio et al., 2008), we considered, for our suppositions, only the isotopic helium from olivines.

In general, the average higher values of $^3\text{He}/^4\text{He}$, compatible with a composite HIMU–MORB signature, were measured in rare “eccentric” eruptions (that is, highly off-axis with respect to the central vents; Rittmann, 1967) (orange symbols in Figure 9) and would be representative of the Etnean mantle source (Correale et al., 2014). On the contrary, more radiogenic values were found in products from central and lateral eruptions, where there are no clear distinctions between recent (purple symbols in Figure 9) and

ancient eruptions (gray and green symbols in Figure 9) with overlapping variabilities. We exclude the fact that the variability of R_c/R_a in Etnean products (4.9–8.2 Ra) could be attributed to degassing processes as the kinetic fractionation of ³He and ⁴He during magma degassing of CO₂-dominated fluids is not possible (Paonita et al., 2012). Otherwise, different isotopic helium could be one consequence of the variable degree of contamination of the magmatic melts during their ascent and/or their stationing in the crustal reservoir. In particular, during “eccentric” eruptions (e.g., 1974, 2001, and 2002–03), the magma, fed by deep dikes and featured by a rapid rise, bypasses the central, shallow, and stalling zones. This would involve a milder crustal contamination and, consequently, an isotopic helium marker less radiogenic than that of magmas that erupted from the more frequent summit or flank eruptions from the central conduit system. Indeed, in this last case, a longer magma residence time in the crustal reservoir results in the enrichment of radiogenic ⁴He. In addition to the ascent velocity, the mass of magma rising in the lithosphere could control the mixing degree with the crustal end-member. In detail, the arrival in the reservoir of abundant deep magma with a high-³He/⁴He signature would increase the isotopic helium of the stored magma which, on the contrary, is characterized by a more marked ³He/⁴He crustal signature.

The data on ³He/⁴He from the 2018 eruption concur with the average values measured during the “routine” Etnean summit and flank activity from central conduits, allowing us to hypothesize the influence of a mild crustal contamination in the isotopic geochemistry of helium controlled by short resident times and/or moderate input volumes of magma.

5.4.2 A comparison between ³He/⁴He in the FIs and in free gases

Volcanic gases furnish important information about deep and shallower degassing zones and can be collected from both the crater and peripheral area (Oppenheimer et al., 2014). At Etna, volcanic degassing is not only measurable from the plume but also from distal gaseous emissions, where the gas migrates toward the surface through soil and mud volcanoes. Volcanic monitoring data, collected between 1996 and 2019 in distal sites of the volcanic edifice (see Figure 9; Caracausi et al., 2003; Paonita et al., 2021), show an R/R_a variability ranging between approximately 6 and 7.4. The data on FIs from the literature (³He/⁴He = 4.9–8.2 Ra) and, in particular, the helium isotopic measurements from this study (³He/⁴He = 6.5–6.6 Ra) are in accordance with the range of free gases from the surface and indicate that a fluid exsolves from a primitive magma with a helium isotopic HIMU–MORB signature of at least 7.3–7.4 Ra (isotopic helium in eccentric eruptions; Correale et al., 2014). It then rises from the depths and variably mixes with fluids from shallower/peripheral types of magmas affected by crustal contamination before ascending as a free gas toward the surface or being entrapped as fluid inclusions in olivines crystallizing in the shallower reservoir. The mixing between crustal and primordial end-members is supported by the mathematical modeling in Paonita et al. (2012). The authors highlighted that the crater fumaroles, and probably the gases released by peripheral vents, are fed by a deep component emerging from the depth, at pressures between 200 and 400 MPa, and a shallower component exsolved at

approximately 130 MPa, which mixes through convective transfers. With a particular reference to the 2018 December eruption, Paonita et al. (2021) affirmed that a long-lasting prelude stage before an eruption, of approximately 6–7 months, followed by pressure buildup in the system at an intermediate depth (5–2 km b.s.L.), affected the magmatic reservoir during this volcanic event. We can, therefore, conclude that during the 2018 December eruption, a magma characterized by a more primordial ³He/⁴He signature of approximately 7.3–7.4 Ra would have risen into the shallower reservoir mixing with locally stored melts and that it took only a few months to modify its primordial signature. Furthermore, evaluating the average ³He/⁴He (6.4 Ra) measured in the FI from the literature dataset (Marty et al., 1994; Nuccio et al., 2008; Correale et al., 2014, this study), the abovementioned mixing process and the timing supposed to modify the isotopic helium signature of the deep end-member with a more superficial one can be extended to most of the eruptions venting from the central conduit.

6 Conclusion

This study focuses on the flank eruption of Etna from 24 to 27 December 2018, which produced both Strombolian explosions at the eruptive fissures and lava flows. In detail, we investigated the major and trace elements of olivines and melt inclusions from pyroclastic products, and this was coupled with the noble gas geochemistry of fluid inclusions in olivines.

We interpreted the resulting geochemical variability as a consequence of mixing between two different magma types which, based on the trace element ratios, are represented by the following:

- (i) The first component recorded a mantle signature that was comparable to magma emitted during the 2001 Upper Vents and 2002 N (Type-1) eruption. This end-member is well-represented by a HIMU + MORB heterogeneous source.
- (ii) The second component featured a more crustal-like fingerprint and was comparable to that emitted during the 2001 Lower Vents and 2002 S (Type-2) eruption.

In detail, a magma batch rose from the deep source into the Etnean reservoir, approximately 6–7 months before the 25 December 2018 eruption, and during its ascent, it was affected by crustal contamination before mixing with the resident HIMU + MORB magma; whereas while the trace element geochemistry records the crustal contamination event, the major elements keep track of the more primitive signature of the deep magma.

We speculate that during the pre-eruptive period (a few months), the two different types of magmas remained in the reservoir long enough to mix their fluid content, as testified by the noble gas geochemistry in FIs, but not that of trace elements that partially preserve their geochemical differences. Although further supporting data are necessary, the comparison between the noble gas literature dataset with the results from our study suggests that this mechanism and timing of contamination could have potentially affected the majority of the Etnean lateral and central eruptions.

Data availability statement

The original contributions presented in the study are included in the article/[Supplementary Material](#); further inquiries can be directed to the corresponding author.

Author contributions

AC: trace element analytical measures, trace element and noble gas data processing, major element, trace element and noble gas data interpretation, and drafting of the manuscript. RC: major element and trace element data interpretation, and drafting of the manuscript. LM: major element analytical measures and major element data processing. AP: major element, trace element, and noble gas data interpretation. SR: drafting of the manuscript. All authors contributed to the article and approved the submitted version.

Acknowledgments

The authors thank Federica Ippolito for her valuable help during sample preparation for major and trace element analyses as part of her M.Sc. thesis and Marco Bracci for his assistance during sample preparation for noble gas analyses. They are also grateful to the careful revision work carried out by the four reviewers and two editors who have undoubtedly improved the manuscript quality.

References

- Achterberg, E., Ryan, C., Jackson, S., and Griffin, W. (2001). Data reduction software for LA-ICP-MS. *Laser Ablation ICP-MS Earth Sci.* 29, 239–243.
- Allard, P., Behncke, B., D'Amico, S., Neri, M., and Gambino, S. (2006). Mount Etna 1993–2005: anatomy of an evolving eruptive cycle. *EarthSci. Rev.* 78, 85–114. doi:10.1016/j.earscirev.2006.04.002
- Alparone, S., Barberi, G., Giampiccolo, E., Maiolino, V., Mostaccio, A., Musumeci, C., et al. (2020). Seismological constraints on the 2018 Mt. Etna (Italy) flank eruption and implications for the flank dynamics of the volcano. *Terra nova.* 32, 334–344. doi:10.1111/ter.12463
- Armienti, P., Innocenti, F., Petrini, R., Pompilio, M., and Villari, L. (1988). Sub-aphyric alkali basalt from Etna: inferences on depth and composition of the source magma. *Rendiconti della Soc. Ital. Mineral. Petrol.* 43, 877–891.
- Armienti, P., Innocenti, F., Petrini, R., Pompilio, M., and Villari, L. (1989). Petrology and Sr-Nd isotope geochemistry of recent lavas from Mt. Etna: bearing on the volcano feeding system. *J. Volcanol. Geoth. Res.* 39, 315–327. doi:10.1016/0377-0273(89)90095-4
- Borzi, A. M., Giuffrida, M., Zuccarello, F., Palano, M., and Viccaro, M. (2020). The Christmas 2018 eruption at Mount Etna: enlightening how the volcano works through a multiparametric inspection. *Geochem. Geophys. Geosystems* 21, e2020GC009226. doi:10.1029/2020GC009226
- Branca, S., and Abate, T. (2017). Current knowledge of Etna's flank eruptions (Italy) occurring over the past 2500 years. From the iconographies of the XVII century to modern geological cartography. *J. Volcanol. Geotherm. Res.* 385, 159–178. doi:10.1016/j.jvolgeores.2017.11.004
- Branca, S., and Del Carlo, P. (2004). "Eruptions of Mt. Etna during the past 3200 years: a revised compilation integrating the historical and stratigraphic records," in *MT. Etna: volcano laboratory, geophys. Monogr. Ser.* (Washington, DC, USA: AGU), 1–27.
- Caracausi, A., Favara, R., Giammanco, S., Italiano, F., Paonita, A., Pecoraino, G., et al. (2003). Mount Etna: geochemical signals of magma ascent and unusually extensive plumbing system. *Geophys. Res. Lett.* 30. doi:10.1029/2002gl015463
- Chester, D. K., Duncan, A. M., Guest, J. E., and Kilburn, C. R. J. (1985). *Mount Etna, the anatomy of a volcano*. London: Chapman and Hall.
- Collins, S. J., Pyle, D. M., and MacLennan, J. (2009). Melt inclusions track pre-eruption storage and dehydration of magmas at Etna. *Geology* 37, 571–574. doi:10.1130/G30040A.1
- Correale, A., Paonita, A., Martelli, M., Rizzo, A., Rotolo, S. G., Corsaro, R. A., et al. (2014). A two-component mantle source feeding Mt. Etna magmatism: insights from the geochemistry of primitive magmas. *Lithos* 184, 243–258. doi:10.1016/j.lithos.2013.10.038
- Correale, A., Rizzo, A., Barry, P. H., Lu, J., and Zheng, J. (2016). Refertilization of lithospheric mantle beneath the Yangtze craton in south-east China: evidence from noble gases geochemistry. *Gondwana Res.* 38, 289–303. doi:10.1016/j.gr.2016.01.003
- Correale, A., Pelorosso, B., Rizzo, A. L., Coltorti, M., Italiano, F., Bonadiman, C., et al. (2019). The nature of the West Antarctic Rift System as revealed by noble gases in mantle minerals. *Chem. Geol.* 524, 104–118. doi:10.1016/j.chemgeo.2019.06.020
- Corsaro, R., Andronico, D., Behncke, B., Branca, S., Caltabiano, T., Ciancitto, F., et al. (2017). Monitoring the December 2015 summit eruptions of Mt. Etna (Italy): implications on eruptive dynamics. *J. Volcanol. Geotherm. Res.* 341, 53–69. doi:10.1016/j.jvolgeores.2017.04.018
- Corsaro, R., Civetta, L., Renzo, V., and Miraglia, L. (2009a). Petrology of lavas from the 2004–2005 flank eruption of Mt. Etna, Italy: inferences on the dynamics of magma in the shallow plumbing system. *Bull. Volcanol.* 71, 781–793. doi:10.1007/s00445-009-0264-z
- Corsaro, R., Renzo, V., Distefano, S., Miraglia, L., and Civetta, L. (2013). Relationship between petrologic processes in the plumbing system of Mt. Etna and the dynamics of the eastern flank from 1995 to 2005. *J. Volcanol. Geotherm. Res.* 251, 75–89. doi:10.1016/j.jvolgeores.2012.02.010
- Corsaro, R. A., Métrich, N., Allard, P., Andronico, D., Miraglia, L., and Fourmentraux, C. (2009b). The 1974 flank eruption of Mount Etna: an archetype for deep dike-fed eruptions at basaltic volcanoes and a milestone in Etna's recent history. *J. Geophys. Res.* 114, B07204. doi:10.1029/2008JB006013
- Corsaro, R. A., and Miraglia, L. (2022). Near real-time petrologic monitoring on volcanic glass to infer magmatic processes during the february–april 2021 paroxysms of the South-East crater, Etna. *Front. Earth Sci.* 10, 828026. doi:10.3389/feart.2022.828026
- Corsaro, R. A., Miraglia, L., and Pompilio, M. (2007). Petrologic evidence of a complex plumbing system feeding the July August 2001 eruption of Mt. Etna, Sicily, Italy. *Bull. Volcanol.* 69, 401–421. doi:10.1007/s00445-006-0083-4
- Corsaro, R. A., and Pompilio, M. (2004). Magma dynamics in the shallow plumbing system of Mt. Etna as recorded by compositional variations in volcanics of recent summit activity (1995–1999). *J. Volcanol. Geotherm. Res.* 137 (1–3), 55–71. doi:10.1016/j.jvolgeores.2004.05.008

This research was carried out in the frame of the IMPACT PROJECT (INGV Department strategic Projects, 2019) WP1, Task 3-Dynamics of magmatic processes.

Conflict of interest

The authors declare that the research was conducted in the absence of any commercial or financial relationships that could be construed as a potential conflict of interest.

Publisher's note

All claims expressed in this article are solely those of the authors and do not necessarily represent those of their affiliated organizations, or those of the publisher, the editors, and the reviewers. Any product that may be evaluated in this article, or claim that may be made by its manufacturer, is not guaranteed or endorsed by the publisher.

Supplementary material

The Supplementary Material for this article can be found online at: <https://www.frontiersin.org/articles/10.3389/feart.2023.1122132/full#supplementary-material>

- Danyushevsky, L. V., Leslie, R. A. J., Crawford, A. J., and Durance, P. (2004). Melt inclusions in primitive olivine phenocrysts: the role of localized reaction processes in the origin of anomalous compositions. *J. Petrol.* 45, 2531–2553. doi:10.1093/petrology/egh080
- Delmelle, P., and Stix, J. (1999). *Encyclopedia of volcanoes*. Amsterdam, Netherlands: Elsevier, 803–815.
- Di Renzo, V., Corsaro, R. A., Miraglia, L., Pompilio, M., and Civetta, L. (2019). Long and short-term magma differentiation at Mt. Etna as revealed by Sr-Nd isotopes and geochemical data. *Earth-Science Rev.* 190, 112–130. doi:10.1016/j.earscirev.2018.12.008
- Dunai, T. J., and Porcelli, D. (2002). “Storage and transport of noble gases in the subcontinental lithosphere,” in *Geochemistry and cosmochemistry*. Editors D. P. Porcelli, C. J. Ballentine, and R. Wieler (Berlin, Boston, USA: De Gruyter), 371–410. doi:10.1515/9781501509056-012
- Ferlito, C., Viccaro, M., Nicotra, E., and Cristofolini, R. (2012). Regimes of magma recharge and their control on the eruptive behaviour during the period 2001–2005 at Mt. Etna volcano. *Bull. Volcanol.* 74, 533–543. doi:10.1007/s00445-011-0537-1
- Ganci, G., Cappello, A., Zago, V., Bilotta, G., Herault, A., and Del Negro, C. (2019). 3D Lava flow mapping of the 17–25 May 2016 Etna eruption using tri-stereo optical satellite data. *Ann. Geophys.* 62 (2), 1–6. doi:10.4401/ag-7875
- Gennaro, E., Iacono-Marziano, G., Paonita, A., Rotolo, S. G., Martel, C., Rizzo, A. L., et al. (2019). Melt inclusions track melt evolution and degassing of Etnean magmas in the last 15 ka. *Lithos* 324–325, 716–732. doi:10.1016/j.lithos.2018.11.023
- Giacomoni, P. P., Coltorti, M., Bryce, J. G., Fahnestock, M. F., and Guitreau, M. (2016). Mt. Etna plumbing system revealed by combined textural, compositional, and thermobarometric studies in clinopyroxenes. *Contributions Mineralogy Petrology* 171, 34. doi:10.1007/s00410-016-1247-7
- Giacomoni, P. P., Ferlito, C., Alesci, G., Coltorti, M., Monaco, C., Viccaro, M., et al. (2012). A common feeding system of the NE and S rifts as revealed by the bilateral 2002/2003 eruptive event at Mt. Etna (Sicily, Italy). *Bull. Volcanol.* 74, 2415–2433. doi:10.1007/s00445-012-0672-3
- Giacomoni, P. P., Ferlito, C., Coltorti, M., Bonadiman, C., and Lanzafame, G. (2014). Plagioclase as archive of magma ascent dynamics on “open conduit” volcanoes: the 2001–2006 eruptive period at Mt. Etna. *Earth-Sciences Rev.* 138, 371–393. doi:10.1016/j.earscirev.2014.06.009
- Giampiccolo, E., Cocina, O., De Gori, P., and Chiarabba, C. (2020). Dyke intrusion and stress-induced collapse of volcano flanks: the example of the 2018 event at Mt. Etna (Sicily, Italy). *Sci. Rep.* 10, 6373. doi:10.1038/s41598-020-63371-3
- Giggenbach, W. F., Sano, Y., and Wakita, H. (1993a). Isotopic composition of helium, and CO₂ and CH₄ contents in gases produced along the New Zealand part of a convergent plate boundary. *Geochimica Cosmochimica Acta* 57, 3427–3455. doi:10.1016/0016-7037(93)90549-c
- Giggenbach, W. F., Sano, Y., and Wakita, H. (1993b). Isotopic composition of helium, and CO₂ and CH₄ contents in gases produced along the New Zealand part of a convergent plate boundary. *Geochimica Cosmochimica Acta* 57, 3427–3455. doi:10.1016/0016-7037(93)90549-c
- Giuffrida, M., and Viccaro, M. (2017). Three years (2011–2013) of eruptive activity at Mt. Etna: working modes and timescales of the modern volcano plumbing system from microanalytical studies of crystals. *Earth Sci. Rev.* 171, 289–322. doi:10.1016/j.earscirev.2017.06.003
- Graham, D. W. (2002). “Noble gas isotope geochemistry of mid-oceanic ridge and ocean island basalts: characterization of mantle source reservoirs,” in *Reviews in mineralogy and geochemistry*. Editors D. P. Porcelli, C. J. Ballentine, and R. Wieler (McLean, VA, USA: GeoScienceWorld), 247–317.
- Gurenko, A. A., and Chaussidon, M. (1995). Enriched and depleted primitive melts included in olivine from Icelandic tholeiites—origin by continuous melting of a single mantle column. *Geochimica Cosmochimica Acta* 59, 2905–2917. doi:10.1016/0016-7037(95)00184-0
- Hilton, D. R., Barling, J., and Wheller, G. E. (1995). Effect of shallow level contamination on the helium isotope systematics of ocean-island lavas. *Nature* 373, 330–333. doi:10.1038/373330a0
- Hofmann, A. W. (1988). Chemical differentiation of the Earth: the relationship between mantle, continental crust, and oceanic crust. *Earth Planet. Sci. Lett.* 90, 297–314. doi:10.1016/0012-821x(88)90132-x
- Jarosewich, E., Nelen, J. A., and Norberg, J. A. (1980). Reference samples for electron microprobe analysis. *Geostand. Newslett.* 4 (1), 43–47. doi:10.1111/j.1751-908x.1980.tb00273.x
- Kahl, M., Chakraborty, S., Costa, F., Pompilio, M., Liuzzo, M., and Viccaro, M. (2013). Compositionally zoned crystals and real-time degassing data reveal changes in magma transfer dynamics during the 2006 summit eruptive episodes of Mt. Etna. *Bull. Volcanol.* 75, 692. doi:10.1007/s00445-013-0692-7
- Kahl, M., Chakraborty, S., Pompilio, M., and Costa, F. (2015). Constraints on the nature and evolution of the magma plumbing system of Mt. Etna volcano (1991–2008) from a combined thermodynamic and kinetic modelling of the compositional record of minerals. *Jour. Petrol.* 56, 2025–2068. doi:10.1093/petrology/egv063
- Kamenetsky, V., and Clochchiatti, R. (1996). Primitive magmatism of Mt. Etna: insights from mineralogy and melt inclusions. *Earth Planet. Sci. Lett.* 142, 553–572. doi:10.1016/0012-821x(96)00115-X
- Le Maitre, R. W. (2002). “Igneous rocks: a classification and glossary of terms,” in *Recommendations of the IUGS subcommission on the systematics of igneous rocks* (Cambridge, England: Cambridge University Press), 236.
- Martelli, M., Bianchini, G., Beccaluva, L., and Rizzo, A. (2011). Helium and argon isotopic compositions of mantle xenoliths from Tallante and Calatrava, Spain. *J. Volcanol. Geotherm. Res.* 185, 172–180. doi:10.1016/j.jvolgeores.2010.11.015
- Martelli, M., Rizzo, A. L., Renzulli, A., Ridolfi, F., Arienzo, I., and Rosciglione, A. (2014). Noble-gas signature of magmas from a heterogeneous mantle wedge: the case of Stromboli volcano (Aeolian Islands, Italy). *Chem. Geol.* 368, 39–53. doi:10.1016/j.chemgeo.2014.01.003
- Marty, B., Trull, T., Lussiez, P., Basile, I., and Tanguy, J. C. (1994). He, Ar, O, Sr and Nd isotope constraints on the origin and evolution of Mount Etna magmatism. *Earth Planet. Sci. Lett.* 126, 23–39. doi:10.1016/0012-821x(94)90240-2
- Métrich, N., Allard, P., Spilliaert, N., Andronico, D., and Burton, M. (2004). 2001 flank eruption of the alkali- and volatile-rich primitive basalt responsible for Mount Etna’s evolution in the last three decades. *Earth Planet. Sci. Lett.* 228, 1–17. doi:10.1016/j.epsl.2004.09.036
- Métrich, N., and Clochchiatti, R. (1996). Sulfur abundance and its speciation in oxidized alkaline melts. *Geochimica Cosmochimica Acta* 60, 4151–4160. doi:10.1016/S0016-7037(96)00229-3
- Métrich, N., and Rutherford, M. J. (1998). Low pressure crystallization paths of H₂O saturated basaltic-hawaiitic melts from Mt Etna: implications for open-system degassing of basaltic volcanoes. *Geochimica Cosmochimica Acta* 62, 1195–1205. doi:10.1016/S0016-7037(98)00048-9
- Miraglia, L. (2012). Caratteristiche del sistema analitico SEM-EDS: valutazione dell’accuratezza e della precisione delle analisi eseguite su standards internazionali di minerali e vetri. https://editoria.ingv.it/archivio_pdf/rapporti/232/pdf/rapporti_233.pdf.
- Mollo, S., Blundy, J., Scarlato, P., De Cristofaro, S. P., Tecchiato, V., Stefano, F., et al. (2018). An integrated P - T - H₂O-lattice strain model to quantify the role of clinopyroxene fractionation on REE+Y and HFSE patterns of mafic alkaline magmas: application to eruptions at Mt. Etna. *Earth-Science Rev.* 185, 32–56. doi:10.1016/j.earscirev.2018.05.014
- Mollo, S., Giacomoni, P. P., Coltorti, M., Ferlito, C., Iezzi, G., and Scarlato, P. (2015). Reconstruction of magmatic variables governing recent Etnean eruptions: constraints from mineral chemistry and P-T-fO₂-H₂O modeling. *Lithos* 212–215, 311–320. doi:10.1016/j.lithos.2014.11.020
- Moretti, R., Métrich, N., Arienzo, I., Di Renzo, V., Aiuppa, A., and Allard, P. (2018). Degassing vs. eruptive styles at Mt. Etna volcano (Sicily, Italy). Part I: volatile stocking, gas fluxing, and the shift from low-energy to highly explosive basaltic eruptions. *Chem. Geol.* 482, 1–17. doi:10.1016/j.chemgeo.2017.09.017
- Nuccio, P. M., Paonita, A., Rizzo, A., and Rosciglione, A. (2008). Elemental and isotope covariation of noble gases in mineral phases from Etnean volcanics erupted during 2001–2005, and genetic relation with peripheral gas discharges. *Earth Planet. Sci. Lett.* 272, 683–690. doi:10.1016/j.epsl.2008.06.007
- Oppenheimer, C., Fischer, T., and Scaillet, B. (2014). “Volcanic degassing: process and impact,” in *Treatise on geochemistry* (Amsterdam, Netherlands: Elsevier), 111–179. doi:10.1016/B978-0-08-095975-7.00304-1
- Paonita, A., Caracausi, A., Marziano-Iacono, G., Martelli, M., and Rizzo, A. (2012). Geochemical evidence for mixing between fluids exsolved at different depths in the magmatic system of Mt Etna (Italy). *Geochimica Cosmochimica Acta* 84, 380–394. doi:10.1016/j.gca.2012.01.028
- Paonita, A., Liuzzo, M., Salerno, G., Federico, C., Bonfanti, P., Caracausi, A., et al. (2021). Intense overpressurization at basaltic open-conduit volcanoes as inferred by geochemical signals: the case of the Mt. Etna December 2018 eruption. *Sci. Adv.* 7, eabg6297 Rittmann, A. (1965). Notizie sull’Etna, Suppl. *Nuovo Cimento* 3 (I), 1117–1123. doi:10.1126/sciadv.abg6297
- Perinelli, C., Mollo, S., Gaeta, M., De Cristofaro, S. P., Palladino, D. M., Armienti, P., et al. (2016). An improved clinopyroxene-based hygrometer for Etnean magmas and implications for eruption triggering mechanisms. *Am. Mineralogist* 101 (12), 2774–2777. doi:10.2138/am-2016-5916
- Pouchou, J. L., and Pichoir, F. (1986). Les éléments très légers en microanalyse X. Possibilités des modèles récents de quantification. *Microsc. Spectrosc. électroniques* 11 (4), 229–250.
- Rittmann, A. (1967). *I vulcani e la loro attività*. Bologna, Cappelli, 1–359.
- Roeder, P. L., and Emslie, R. F. (1970). Olivine-liquid equilibrium. *Contrib. Mineral. Petrol.* 29, 275–289. doi:10.1007/bf00371276
- Rose-Koga, E., Bouvier, A. S., Gaetani, G., Wallace, P. J., Allison, C. M., Andry, J. A., et al. (2021). Silicate melt inclusions in the new millennium: a review of recommended practices for preparation, analysis, and data presentation. *Chem. Geol.* 570, 120145. doi:10.1016/j.chemgeo.2021.120145
- Rudnick, R. L., and Gao, S. (2004). “Composition of the continental crust,” in *Treatise on geochemistry*. Editor R. L. Rudnick (New York, NY, USA: Elsevier), 1–64.
- Ryan, M. P. (1988). The mechanics and three-dimensional internal structure of active magmatic systems: kilauea Volcano, Hawaii. *J. Geophys. Res.* 93, 4213–4248. doi:10.1029/JB093iB05p04213

- Schiavi, F., Rosciglione, A., Kitagawa, H., Kobayashi, K., Nakamura, E., Nuccio, P. M., et al. (2015). Geochemical heterogeneities in magma beneath Mount Etna recorded by 2001–2006 melt inclusions. *Geochem. Geophys. Geosyst.* 16, 2109–2126. doi:10.1002/2015GC005786
- Shaw, A. M., Hilton, D. R., Fisher, T. P., Walker, J. A., and De Leeuw, G. A. M. (2006). Helium isotope variations in mineral separates from Costa Rica and Nicaragua: assessing crustal contributions, timescale variations and diffusion-related mechanisms. *Chem. Geol.* 230, 124–139. doi:10.1016/j.chemgeo.2005.12.003
- Sobolev, A. V. (1996). Melt inclusions in minerals as a source of principal petrological information. *Petrology* 4, 228–239.
- Sobolev, A. V., Hofmann, A. W., and Nikogosian, I. K. (2000). Recycled oceanic crust observed in ‘ghost plagioclase’ within the source of Mauna Loa lavas. *Nature* 404, 986–990. doi:10.1038/35010098
- Sobolev, A. V., and Shimizu, N. (1993). Ultra-depleted primary melt included in an olivine from the Mid-Atlantic Ridge. *Nature* 363, 151–154. doi:10.1038/363151a0
- Spilliaert, N., Allard, P., Métrich, N. A., and Sobolev, V. (2006). Melt inclusion record of the conditions of ascent, degassing, and extrusion of volatile-rich alkali basalt during the powerful 2002 flank eruption of Mount Etna (Italy). *J. Geophys. Res.* 111, B04203. doi:10.1029/2005JB003934
- Sun, W., and McDonough, W. (1989). *Chemical and isotopic systematics of oceanic basalts: implications for mantle composition and processes*. London: Geological Society. doi:10.1144/GSL.SP.1989.042.01.19
- Tanguy, J. C. (1980). L’Etna: étude pétrologique et paléomagnétique; implications volcanologiques. *Tesi Dottor., Univ. Parigi* 6, 618.
- Tonarini, S., Armienti, P., D’Orazio, M., and Innocenti, F. (2001). Subduction-like fluids in the genesis of the Mt Etna magmas: evidence from boron isotopes and fluid mobile elements. *Earth Planet. Sci. Lett.* 5989, 1–13. doi:10.1016/S0012-821X(01)00487-3
- Toplis, M. J. (2005). The thermodynamics of iron and magnesium partitioning between olivine and liquid: criteria for assessing and predicting equilibrium in natural and experimental systems. *Contrib. Mineral. Petrol.* 149, 22–39. doi:10.1007/s00410-004-0629-4
- Viccaro, M., and Cristofolini, R. (2008). Nature of mantle heterogeneity and its role in the short term geochemical and volcanological evolution of Mt Etna (Italy). *Lithos* 105, 272–288. doi:10.1016/j.lithos.2008.05.001
- Viccaro, M., Ferlito, C., Cortesogno, L., Cristofolini, R., and Gaggero, L. (2006). Magma mixing during the 2001 event at Mount Etna (Italy): Effects on the eruptive dynamics. *J. Volcanol. Geotherm. Res.* 149, 139–159. doi:10.1016/j.jvolgeores.2005.06.004
- Viccaro, M., Giacomoni, P., Ferlito, C., and Cristofolini, R. (2010). Dynamics of magma supply at Mt. Etna Volcano (Southern Italy) as revealed by textural and compositional features of plagioclase phenocrysts. *Lithos* 116, 77–91. doi:10.1016/j.lithos.2009.12.012
- Viccaro, M., Zuccarello, F., Cannata, A., Palano, M., and Gresta, S. (2016). How a complex basaltic volcanic system works: constraints from integrating seismic, geodetic, and petrological data at Mount Etna volcano during the July–August 2014 eruption. *J. Geophys. Res. Solid Earth* 121, 5659–5678. doi:10.1002/2016JB013164
- Wadge, G. (1980). “Flank fissures of Etna and the surface expressions of magmatic conduits,” in *United Kingdom research on Mount Etna 1977–79* (London: R. Soc.), 27–30.
- White, M. J. (2005). *Geochemistry*. Hoboken, New Jersey, United States: John Wiley and Sons, 496.
- Woodhead, J. D. (1996). Extreme HIMU in an oceanic setting: the geochemistry of Mangaia Island (Polynesia), and temporal evolution of the Cook-Austral hotspot. *J. Volcanol. Geoth. Res.* 72, 1–19. doi:10.1016/0377-0273(96)00002-9
- Zuccarello, F., Schiavi, F., and Viccaro, M. (2021). Magma dehydration controls the energy of recent eruptions at Mt. Etna volcano. *Terra nova*. 33, 423–429. doi:10.1111/ter.12527
- Zuccarello, F., Schiavi, F., and Viccaro, M. (2022). The eruption run-up at Mt. Etna volcano: constraining magma decompression rates and their relationships with the final eruptive energy. *Earth Planet. Sci. Lett.* 597, 117821. doi:10.1016/j.epsl.2022.117821